The Astrophysical Journal, 660: L133–L136, 2007 May 10

ARCSECOND-SCALE KINEMATIC AND CHEMICAL COMPLEXITY IN CEPHEUS A EAST

C. L. Brogan,[1] C. J. Chandler,[1] T. R. Hunter,[1] Y. L. Shirley,[2] and A. P. Sarma[3]

Received 2006 December 4; accepted 2007 March 23; published 2007 April 17

ABSTRACT

We present results from Submillimeter Array (SMA) observations of the star-forming region Cepheus A East at ~340 GHz (875 μm) with 0.7″–2″ resolution. At least four compact submillimeter continuum sources have been detected as well as a rich forest of hot core line emission. Two kinematically, chemically, and thermally distinct regions of molecular emission are present in the vicinity of the HW2 thermal jet, both spatially distinct from the submillimeter counterpart to HW2. We propose that this emission is indicative of multiple protostars rather than a massive disk as reported by Patel et al.

Subject headings: ISM: individual (Cepheus A) — ISM: lines and bands — ISM: molecules

1. INTRODUCTION

The Cepheus A East (hereafter Cep A) star-forming region lies at a distance $D \sim 725$ pc and has $L_{\rm bol} \sim 2.2 \times 10^4\ L_\odot$, consistent with a cluster of B0.5 or later stars (Blaauw et al. 1959; Sargent 1979; Mueller et al. 2002). At centimeter wavelengths, Cep A consists of several compact sources called HW1, HW2, …, HW9, which lie along a roughly inverted Y-like structure (e.g., Hughes & Wouterloot 1984; Garay et al. 1996). It is currently unclear how many of these compact ionized structures correspond to individual protostars. For example, much of the centimeter-wavelength emission from the HW2 region is due to a bipolar thermal jet rather than a Strömgren sphere (Rodríguez et al. 1994; Curiel et al. 2006).

A wide range of other signposts of ongoing star formation have been observed in Cep A, including several outflow components (e.g., Codella et al. 2005 and references therein); however, the locations of the powering sources remain uncertain. On smaller size scales, copious OH, H_2O, and CH_3OH maser emission has been detected toward several of the centimeter-wavelength sources (Vlemmings et al. 2006 and references therein). Patel et al. (2005) report the detection of a massive molecular gas and dust disk toward the HW2 source from Submillimeter Array[4] (SMA) observations of methyl cyanide.

In this Letter, we present new and archival SMA 345 GHz observations toward Cep A (including those of Patel et al. 2005), concentrating on the continuum data and the spatial, kinematic, and temperature information provided by the wealth of spectral lines; complete details of the spectral line results will be presented in a future paper. Our observations and results are presented in § 2 and are discussed in § 3.

2. OBSERVATIONS AND RESULTS

The SMA observing parameters are provided in Table 1. The data were taken with a channel width of 0.8125 MHz (~0.7 km s^{-1}), except for the archival data, which have 8 times poorer spectral resolution across most of the band [the $CH_3CN(18–17)$ $K = 0–3$ lines were observed with ~0.7 km s^{-1} resolution]. All five epochs employed seven antennas. The data were calibrated using the MIRIAD software package. The quasars BL Lac and 3C 454.3 were used for phase calibration. 3C 454.3, Uranus, and Saturn were used for bandpass calibration. Comparison of the amplitude calibration (from the quasars) applied to Uranus versus a model of its baseline-dependent flux density suggests that the Cep A amplitude calibration is accurate to within ~15%.

Continuum subtraction, imaging, deconvolution, and self-calibration were carried out in AIPS. After extracting the continuum using line-free channels in the *u-v* data, the continuum for each observation/sideband were separately self-calibrated; the derived phase and amplitude corrections were also applied to the line data sets. The spectral line data were Hanning-smoothed during imaging to produce a final spectral resolution of ~1.4 km s^{-1} (except for the archival SMA data set with 5.9 km s^{-1} spectral resolution). To create the highest possible sensitivity continuum image, all of the final continuum data sets were combined in the *u-v* plane and imaged.

2.1. *Cep A Submillimeter Continuum*

Figure 1*a* shows the combined naturally weighted 875 μm SMA continuum image with a beam of 1.3″ × 1.1″ and integrated flux density of 7.7 Jy; the rms noise is 13 mJy beam^{-1}. The peak of the single-dish submillimeter source (see, e.g., Mueller et al. 2002) has been resolved for the first time into a number of distinct components. Archival 2002 Very Large Array[5] (VLA) 3.6 cm continuum contours are also shown for comparison. While there is rough agreement between the peak 875 μm continuum emission and the well-known ionized thermal jet HW2 (e.g., Rodríguez et al. 1994; Garay et al. 1996), there is excess emission to the northwest of HW2 suggestive of additional unresolved structure.

In order to better compare the morphology of the centimeter and submillimeter emission, we have also created a superuniform-weighted image using baselines >40 kλ, resulting in a beam size of 0.8″ × 0.7″. To further delineate the morphology of the emission in the vicinity of HW2, in Figure 1*b*, we present the superuniform-weighted image restored with a 0.6″ beam (equivalent to 1.8 times the longest baseline sampled) that emphasizes the locations of the clean components. Figure 1*b* re-

[1] National Radio Astronomy Observatory, Charlottesville, VA 22903; cbrogan@nrao.edu.

[2] University of Arizona, Tucson, AZ; Bart J. Bok Fellow.

[3] Physics Department, DePaul University, Chicago, IL.

[4] The Submillimeter Array is a joint project between the Smithsonian Astrophysical Observatory and the Academia Sinica Institute of Astronomy and Astrophysics.

[5] The National Radio Astronomy Observatory operates the Very Large Array and is a facility of the National Science Foundation operated under a cooperative agreement by Associated Universities, Inc.

TABLE 1
SMA Observing Parameters

Date	*u-v* Range (kλ)	t_{int} (hr)	USB/LSB[a] (GHz)	Line Beam[b] (arcsec; deg)
2004 Aug 30[c]	20–190	5.7	331.4/...	0.9 × 0.8; 77
2004 Sep 26, Oct 18	14–130	5.0	343.0/333.0	1.9 × 1.2; 71
2005 Oct 5, 7	10–80	4.1	346.6/336.6	2.0 × 1.9; 33

[a] Approximate center frequency of 2 GHz–wide sidebands. USB = upper sideband; LSB = lower sideband.
[b] Synthesized beam and position angle of the USB line data.
[c] Archival Patel et al. (2005) data, only the upper sideband was analyzed.

veals the presence of at least two distinct submillimeter sources in the vicinity of HW2, HW2-SMA and SMA1, in addition to an extension northwest of HW2-SMA that we denote SMA2 (see § 3). A weak extension south of HW2-SMA (denoted SMA3) is also visible, which may be a submillimeter counterpart to the low-mass protostar VLA-R5 (Curiel et al. 2002). The combined morphology of HW2-SMA, SMA2, and SMA3 is the structure reported by Patel et al. (2005) as a dust disk; their Figure 1 with ∼0.75″ resolution also shows that the centroid of submillimeter emission is not centered on the axis of the HW2 jet. The HW2-SMA 875 μm continuum peak is within 0.1″ of the proposed location of the powering source of the HW2 thermal jet based on high-resolution (0.05″) 7 mm VLA data (Curiel et al. 2006), which is well within our absolution position uncertainty of 0.15″. Two additional submillimeter cores are detected to the south of HW2, one coincident with the centimeter-wavelength source HW3c (denoted HW3c-SMA) and another located at the northeast tip of the centimeter-wavelength source HW3b (designated SMA4). No distinct compact 875 μm counterparts to HW8, HW9, HW3a, HW3b, or HW3d are detected in the SMA data.

2.2. *Cep A Hot Core Line Emission*

Within the 8 GHz of total bandwidth observed (Table 1), we detect more than 20 distinct species along with a number of their isotopologues. A few transitions with low-excitation energies [^{12}CO(3–2), CS(7–6), and H^{13}CO$^+$(4–3)] show extended emission over the full primary beam (∼36″) corresponding to the previously studied outflows (see, e.g., Codella et al. 2005). However, the emission from most species is restricted to compact regions (≲2″) that coincide with the submillimeter continuum emission (Fig. 1*b*). At 1″–2″ resolution (Table 1), the species exhibiting compact emission in the vicinity of HW2 are strongest at one of two distinct velocities: −5.0 ± 0.5 or −10.5 ± 0.5 km s^{-1} (Figs. 1*b*–1*d*; see also Codella et al. 2006). These two kinematic features are also spatially distinct. Without exception, molecules that are strongest at ∼−10.5 km s^{-1} have peak positions ∼0.25″ (200 AU) east-northeast of HW2-SMA (we denote this position HW2-NE), and molecules that are strongest at ∼−5 km s^{-1} peak at the position of SMA2. Although this dichotomy exists for all observed species, a few abundant high-density tracers like CH_3CN and C^{34}S show emission of nearly equal strength toward both positions (Figs. 1*c* and 1*d*).

Using 3 mm Plateau de Bure Interferometer (PdBI) data, Martín-Pintado et al. (2005) also find that SO_2 emission peaks to the east-northeast of HW2 at a velocity of ∼−10.5 km s^{-1} and suggest that this emission is due to a distinct intermediate-mass protostar; the SMA and PdBI SO_2 positions agree to within the absolute position uncertainty of 0.15″. This result has recently been confirmed by the VLA detection of SO_2 emission and weak 7 mm continuum emission at the position of HW2-NE (Jiménez-Serra et al. 2007). In an extensive PdBI spectral line study, C. Comito et al. (2007, in preparation) also find strong spatial, chemical, and kinematic differentiation in general agreement with the SMA results. The two velocity components at ∼−5 and ∼−10.5 km s^{-1} have also been observed in single-dish H_2CS, CH_3OH, and HDO data with resolutions ranging from 10″ to 30″ (Codella et al. 2006). The single-dish emission from both velocity components is extended. Our SMA data are insensitive to spatial structures ≳15″, but it seems likely that SMA2 is associated with the larger scale ∼−5 km s^{-1} component.

For CH_3OH toward SMA2 (at ∼−5 km s^{-1}), and SO_2 and HC_3N toward HW2-NE (at ∼−10.5 km s^{-1}), we have measured enough transitions to construct rotation diagrams (Fig. 2; see Goldsmith & Langer 1999). Emission from the two velocity

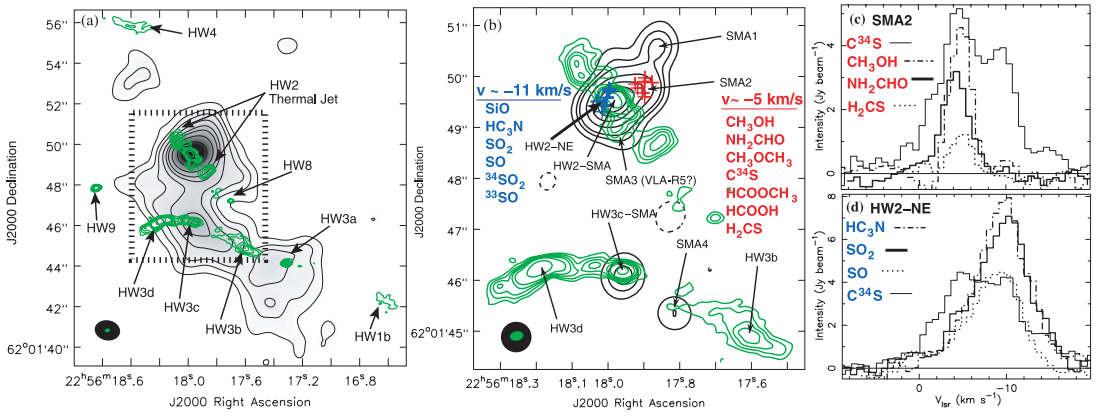

FIG. 1.—(*a*) Combined SMA 875 μm continuum image (*gray scale and black contours*) with a resolution of 1.3″ × 1.0″ (P.A. = 79°) and contour levels of −40, 40 (3 σ), 80, 120, 200, 300, 400, 600, 1000, and 1600 mJy beam^{-1}. This image has not been corrected for primary-beam attenuation. Green VLA 3.6 cm contours at 0.06 (3 σ), 0.12, 0.2, 0.3, 0.4, 0.5, and 1.5 mJy beam^{-1} and 0.23″ resolution are superposed. The region shown in panel *b* is indicated by the dashed box. (*b*) Superuniform-weighted 875 μm contour map (*black*) created using baselines longer than 40 kλ and restored with a 0.6″ beam; the contour levels are −50, 50 (4 σ), 100, 150, 300, 500, 700, and 900 mJy beam^{-1}. The green contours are the same as in panel *a*. The synthesized beams are shown in the lower left. Colored crosses mark the peak positions of the molecular species listed. Prominent centimeter-λ and submillimeter sources are also labeled. Also shown are sample spectral line profiles from the positions indicated on panel *b* for (*c*) SMA2 and (*d*) HW2-NE. The displayed transitions are C^{34}S(7–6), $CH_3OH(14_{7,8}\,A^{\pm}–15_{6,9}\,A^{\pm})$, $NH_2CHO(16_{2,15}–15_{2,14})$, $H_2CS(10_{0,10}–9_{0,9})$, HC_3N(38–37), $SO_2(16_{7,9}–17_{6,12})$, and $SO(11_{10}–10_{10})$. Note that at the spectral line angular resolution of these transitions (∼2″), the two positions are not completely independent.

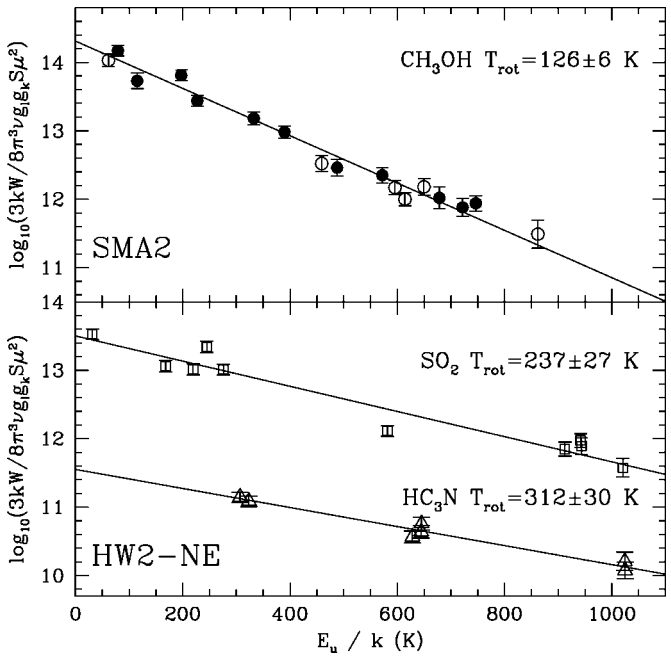

FIG. 2.—Rotation diagrams for CH_3OH *A* (*filled circles*) and *E* (*open circles*) transitions toward SMA2 and for SO_2 (*open squares*) and HC_3N (*open triangles*) toward HW2-NE (see Fig. 1*b*). The CH_3OH and SO_2 data have been corrected for optical depth effects.

components is well separated, even though the emission is not completely spatially resolved by our observations (Figs. 1*c* and 1*d*). The CH_3OH and SO_2 data have been corrected for optical depth effects by first estimating the opacity of one transition using a less abundant isotopologue and assuming Galactic abundance ratios of $^{12}C/^{13}C = 70$ and $^{32}S/^{34}S = 23$ (Milam et al. 2005; Chin et al. 1996 and references therein). Then, assuming LTE, the other transitions were corrected using the formalism described in Sutton et al. (2004). The CH_3OH optical depths are significant (up to 28.2); the SO_2 optical depth is more moderate (up to 2.4). A moderate optical depth in the lower lying HC_3N lines is also possible (see, e.g., Wyrowski et al. 1999), correction for which would yield an HC_3N T_{rot} more consistent with SO_2. Three of the lower energy *A*-type transitions of CH_3OH and the two lowest energy transitions of HC_3N are also detected toward HW3c-SMA and SMA4; rotation diagram analysis for these two submillimeter cores yield $T_{rot} = 65 \pm 25$ K.

In addition to the kinematic and chemical dichotomy between SMA2 and HW2-NE, their T_{rot} differ by more than 100 K. Both values of T_{rot} (Fig. 2) are significantly larger than reported by Torrelles et al. (1999) based on ~1″ resolution VLA NH_3 data ($T_{rot} = 30$–50 K), influenced by their reported nondetection of NH_3 (4, 4) ($E_u/k = 202$ K). An NH_3 (4, 4) integrated intensity image from our reduction of these archival data is shown in Figure 3; emission is clearly detected toward both HW2-NE and SMA2. A new analysis of the NH_3 data gives T_{rot} within a factor of 2 of those reported here. Our T_{rot} values are also larger than those estimated by Patel et al. (2005; 25–75 K), although the sense of the temperature gradient is in agreement (i.e., warmer in the east than in the west). Although Patel et al. (2005) report that CH_3CN(18–17) is not detected above $K = 3$, our reduction of their archival SMA data detects CH_3CN up through $K = 8$ ($E_u/k = 607$ K; $K = 6$ is shown in Fig. 3), and we find similar T_{rot} values to those shown in Figure 2. Using 30 m data, Martín-Pintado et al. (2005) derived $T_{rot} \sim 150$ K for 3 mm SO_2 and HC_3N transitions toward HW2-NE; however, beam dilution may well play a role in this single-dish result.

3. DISCUSSION

The observed distribution of submillimeter continuum emission in the immediate vicinity of HW2 (±0.5″) allows for two possible interpretations: a single elongated structure or two (or more) marginally resolved individual sources. Although the kinematic dichotomy between the positions labeled HW2-NE and SMA2 (Fig. 1*b*) could be interpreted as a velocity gradient across a continuous structure (e.g., Patel et al. 2005), the dramatic chemical and thermal differentiation demonstrated by our multispecies analysis is difficult to explain with this picture. Chemical and thermal gradients might be expected in the radial and vertical directions within a protostellar disk, but such dramatic azimuthal asymmetries are more difficult to conceive in a single-source scenario. We also note that beyond a velocity gradient, the kinematic evidence for a Keplerian rotating disk is quite weak. For example, the weakness of the emission at the central HW2 position in position-velocity (P-V) diagrams such as those in Patel et al. (2005) and in our own data, but not shown, are inconsistent with theoretical expectations unless a central hole is invoked (e.g., Richer & Padman 1991). Even with this modification, it remains difficult to explain the unequal position offsets of the two velocity peaks from the HW2 stellar position (see NH_3 in Fig. 3 and the $K = 3$ P-V diagram of Patel et al. 2005). In contrast, the presence of multiple sources at different velocities naturally explains the observed behavior. We therefore favor the multiple-source hypothesis (see also Martín-Pintado et al. 2005), with at least three sources in the vicinity of HW2 (HW2-SMA, HW2-NE, and SMA2). The remaining discussion proceeds with this interpretation.

Table 2 summarizes the properties of the submillimeter cores

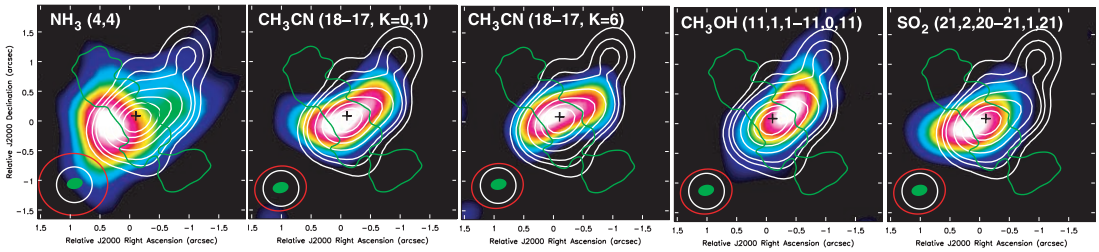

FIG. 3.—Integrated intensity images (over the full width of the observed emission) of archival VLA NH_3 (4, 4) data with 1.1″ × 1.0″ resolution and archival SMA data with 0.87″ × 0.75″ resolution. White 875 μm contours from Fig. 1*b* and a green 0.6 mJy beam^{-1} 3.6 cm contour are superposed. The black cross shows the proposed location of the star powering the HW2 thermal jet (Curiel et al. 2006). The beams are shown in the lower left, and the reference position is $22^h56^m17.998^s$, 62°01′49.50″ (J2000).

TABLE 2
DERIVED PARAMETERS OF SUBMILLIMETER CORES

Name	R.A., Decl.[a] (s, arcsec)	S_ν[b] (Jy beam^{-1})	T_b (K)	T_d (K)	$M_{\rm gas}$ ($M_\odot$)
SMA1	17.873, 50.56	0.28	5.0	20–100	1.0–0.1
SMA2	17.927, 49.74	0.80	14.4	115–135	0.32–0.27
HW2-SMA	17.999, 49.43	1.17	21.0	40–100	2.0–0.6
HW3c-SMA	17.949, 46.07	0.25	4.5	40–90	0.3–0.1
SMA4	17.820, 45.33	0.16	2.9	40–90	0.2–0.1

[a] J2000 coordinates added to $22^{\rm h}56^{\rm m}$, 62°01′; the relative and absolute position uncertainties are better than 0.02″ and 0.15″, respectively.
[b] Using superuniform-weighted image with restoring beam 0.84″ × 0.70″.

identified in Figure 1*b* (excluding SMA3). The gas masses were estimated using

$$M_{\rm gas} = \frac{RS_\nu D^2 \tau_{\rm dust}}{B(\nu, T_d)\kappa(\nu)[1 - \exp(-\tau_{\rm dust})]}, \quad (1)$$

and assuming a gas-to-dust ratio $R = 100$, $D = 725$ pc, and a dust opacity $\kappa_{875\,\mu{\rm m}} = 1.84$ cm^2 g^{-1} extrapolated from Ossenkopf & Henning (1994) for thin ice mantles and density 10^6 cm^{-3}. Values for the peak flux density S_ν (none of the cores appear to be resolved), the continuum brightness temperature (T_b), and the range of assumed dust temperatures (T_d) are also listed in Table 2. The $M_{\rm gas}$ have been corrected for the continuum opacity calculated from $\tau_{\rm dust} = -\ln[1 - (T_b/T_d)]$.

The derived masses are very sensitive to the assumed temperatures (Table 2). For SMA2, HW3c, and SMA4, we have used the range of dust temperatures from rotation diagram analysis (§ 2.2). Temperatures for HW2-SMA and SMA1 are difficult to estimate due to the proximity of strong emission from HW2-NE and SMA2. No species peak at the position of HW2-SMA, suggesting that it is not very warm (i.e., compared to SMA2 or HW2-NE), although its association with the strong bipolar jet suggests that it is unlikely to be very cold either. Thus, we have assumed a moderate-temperature range of 40–100 K for HW2-SMA. Since SMA1 is lacking both a centimeter-wavelength counterpart and any distinct line emission, we assume a cooler lower limit (20 K). With these assumptions, the total gas masses are fairly low, ranging from 0.1 to 2.0 $M_\odot$. If these are preprotostellar cores, this result implies that a *massive* star will not form; if, however, an embedded star is present (almost certainly true for HW2-SMA), these masses are consistent with typical values observed for intermediate-mass protostellar disks (e.g., Hamidouche et al. 2006).

No compact submillimeter emission corresponding to HW8, HW9, HW3a, HW3b, or HW3d is detected. HW3a, HW8, and HW9 are variable at centimeter wavelengths and are thought to be low-mass pre–main-sequence stars (e.g., Hughes 1988; Garay et al. 1996); hence, it is unsurprising that any submillimeter emission is below our 3 σ detection threshold of 40 mJy beam^{-1}. Based in part on the detection of very compact (0.1″) 2 cm emission toward HW3d (Hughes 1988), Garay et al. (1996) suggest that HW3d contains its own internal energy source but also has thermal jetlike extended centimeter-wavelength emission. Given its lack of distinct submillimeter continuum or line emission, we suggest instead that HW3d is a one-sided ionized jet emanating from HW3c-SMA (see Fig. 1*b*). HW3b is consistent with being a one-sided jet emanating from SMA4 or possibly the counterjet to HW3d (also see Garay et al. 1996).

We detect at least five submillimeter sources (HW2-SMA, SMA1, SMA2, HW3c-SMA, and SMA4) within a projected radius of 4″ (2900 AU). If the five low-mass sources HW3a, HW8, HW9, VLA-R5, and VLA-R4 (Hughes 1988; Curiel et al. 2002) are included and equal clustering in the perpendicular dimension is assumed, then the implied protostellar density is 5.7×10^5 pc^{-3}. This approaches the minimum theoretical value (10^6 pc^{-3}) needed to test the induced binary merger hypothesis proposed as a formation mechanism for the most massive stars (Bonnell & Bate 2005).

We thank the SMA staff for their assistance. This research used the JPL (http://spec.jpl.nasa.gov) and Cologne (http://www.ph1.uni-koeln.de/vorhersagen) molecular spectroscopy databases. This work has been partially supported by start-up funds to A. P. S. at DePaul University.

REFERENCES

Blaauw, A., Hiltner, W. A., & Johnson, H. L. 1959, ApJ, 130, 69
Bonnell, I. A., & Bate, M. R. 2005, MNRAS, 362, 915
Chin, Y.-N., Henkel, C., Whiteoak, J. B., Langer, N., & Churchwell, E. B. 1996, A&A, 305, 960
Codella, C., Bachiller, R., Benedettini, M., Caselli, P., Viti, S., & Wakelam, V. 2005, MNRAS, 361, 244
Codella, C., Viti, S., Williams, D. A., & Bachiller, R. 2006, ApJ, 644, L41
Curiel, S., et al. 2002, ApJ, 564, L35
———. 2006, ApJ, 638, 878
Garay, G., Ramirez, S., Rodríiguez, L. F., Curiel, S., & Torrelles, J. M. 1996, ApJ, 459, 193
Goldsmith, P. F., & Langer, W. D. 1999, ApJ, 517, 209
Hamidouche, M., Looney, L. W., & Mundy, L. G. 2006, ApJ, 651, 321
Hughes, V. A. 1988, ApJ, 333, 788
Hughes, V. A., & Wouterloot, J. G. A. 1984, ApJ, 276, 204
Jiménez-Serra, I., Martín-Pintado, J., Rodríguez-Fraco, A., Chandler, C., Comito, C., & Schilke, P. 2007, ApJ, submitted
Martín-Pintado, J., Jiménez-Serra, I., Rodríguez-Franco, A., Martín, S., & Thum, C. 2005, ApJ, 628, L61
Milam, S. N., Savage, C., Brewster, M. A., Ziurys, L. M., & Wyckoff, S. 2005, ApJ, 634, 1126
Mueller, K. E., Shirley, Y. L., Evans, N. J., & Jacobson, H. R. 2002, ApJS, 143, 469
Ossenkopf, V., & Henning, T. 1994, A&A, 291, 943
Patel, N. A., et al. 2005, Nature, 437, 109
Richer, J. S., & Padman, R. 1991, MNRAS, 251, 707
Rodríguez, L. F., Garay, G., Curiel, S., Ramirez, S., Torrelles, J. M., Gomez, Y., & Velazquez, A. 1994, ApJ, 430, L65
Sargent, A. I. 1979, ApJ, 233, 163
Sutton, E. C., Sobolev, A. M., Salii, S. V., Malyshev, A. V., Ostrovskii, A. B., & Zinchenko, I. I. 2004, ApJ, 609, 231
Torrelles, J. M., Gómez, J. F., Garay, G., Rodríguez, L. F., Miranda, L. F., Curiel, S., & Ho, P. T. P. 1999, MNRAS, 307, 58
Vlemmings, W. H. T., Diamond, P. J., van Langevelde, H. J., & Torrelles, J. M. 2006, A&A, 448, 597
Wyrowski, F., Schilke, P., & Walmsley, C. M. 1999, A&A, 341, 882